Efficient Numerical Computation of Dispersion Diagrams for Glide-Symmetric Periodic Structures with a Hexagonal Lattice

Efficient Numerical Computation of Dispersion Diagrams for Glide-Symmetric Periodic Structures with a Hexagonal Lattice

M. Petek*¶, J. A. Tobon Vasquez*, G. Valerio†‡, F. Mesa§, O. Quevedo-Teruel¶, F. Vipiana*
*Dept. of Electronics and Telecommunications, Politecnico di Torino, 10129, Torino, Italy
martin.petek@polito.it**, jorge.tobon@polito.it, francesca.vipiana@polito.it
†Sorbonne Université, CNRS, Laboratoire de Génie Électrique et Électronique de Paris (GeePs), 75252, Paris, France
‡Université Paris-Saclay, CentraleSupélec, CNRS, GeePs, 91192, Gif-sur-Yvette, France, guido.valerio@sorbonne-universite.fr
§Dept. Física Aplicada 1, Universidad de Sevilla, Seville, Spain, mesa@us.es
¶KTH Royal Institute of Technology, Division of Electromagnetic Engineering, 11428, Stockholm, Sweden, oscarqt@kth.se
***corresponding author*

***Abstract*—In this work, we present a modeling methodology to solve the eigenvalue problem for periodic structures with a hexagonal lattice. The method is based on the previously proposed multi-modal transfer matrix method, which is a hybrid method that takes into account the coupling between the multiple modes of the ports surrounding the single unit cell. Commercial software can be used to obtain the generalized scattering parameters which are subsequently applied to set up and solve the eigenvalue problem of the periodic structure. This approach has the ability to obtain complex solutions and thus makes it possible to analyze the attenuation in the stopbands. Here, we extend the multimodal transfer matrix method to the efficient solution of the resulting eigenvalue problem for the case of a hexagonal lattice, detailing the selection of the appropriate supercells and the appropriate irreducible Brillouin zones. Two types of structures are analyzed: a mirror-symmetric structure and a glide-symmetric structure. Very good agreement is obtained with commercial software, limited to the real part of the dispersion diagrams.**

***Index Terms*—eigenmode analysis, electromagnetics, glide symmetry, hexagonal lattice, periodic structures, metasurfaces, numerical methods.**

I. Introduction

Periodic surfaces have long been a topic of interest for the antenna community. They can be employed to tailor the propagation of waves by synthesizing artificial surfaces or metasurfaces that can implement an equivalent refractive index in a meta-waveguide, or block the propagation of waves in an electromagnetic band gap (EBG) structure. Guiding structures based on metasurfaces can be constituted by parallel-plates waveguides (PPW) with periodic inclusions in the plates, bounding the electromagnetic wave between them, and controlling their propagation features by means of their periodicity. Recently, the introduction of glide symmetry into periodic structures has been a topic of intense research [1]–[4], since they can provide a significant improvement of several properties compared to conventional periodic structures, in terms of reduced frequency dispersion, stopband rejection, stable anisotropy, matching properties [5]. A glide-symmetric structure is defined as being invariant with respect to a translation of half a period and a mirroring [6], [7]. The characteristics of periodic structures are usually represented by dispersion diagrams, which are generated through numerical simulations. Many different methods have been used, including commercial software [8], mode matching [2], [4], the multi-modal transfer matrix method (MMTMM) [9], [10], method of moments [11], [12], and the finite element method [13]. However, most of the work to date, apart from a few recent papers [13]–[15], has been devoted to the examination and comprehension of rectangular lattices. In [13], the authors study the surface modes of an open structure while in [14], [15], the modeling of hexagonal lattice is carried out by means of commercial software, which does not directly provide the attenuation in stopbands.

In this work, we develop the MMTMM [9] to analyze closed periodic structures with a hexagonal lattice. The MMTMM is a hybrid method that is capable of obtaining complex modes, including stopband attenuation. We use this method to examine a unit cell with mirror and glide symmetry. This is the first time this method has been developed and used for the mode analysis of hexagonal lattice periodic structures. The presented analysis and discussion provide key insights into the behavior and use of these structures.

II. Brillouin zones of hexagonal cells

In this Section we describe the two periodic structures studied, a mirror-symmetric one and a glide-symmetric one, and their Brillouin diagrams. The numerical values of the relevant geometric parameters described below are the same for the two structures, and are chosen such that, in the glide-symmetric unit cell, the start of the stopband is about 30 GHz and the stopband bandwidth is maximized.

Before applying the MMTMM, it is essential to determine the Brillouin zones that are associated with the unit cells of

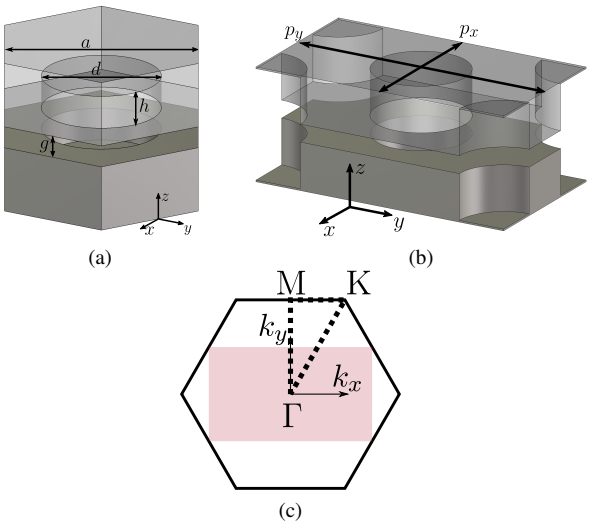

Fig. 1. Geometries of the mirror-symmetric structure: (a) Primitive unit cell and (b) the supercell. (c) The boundary of the first Brillouin zone (full line) and the irreducible Brillouin zone (dashed line) of the primitive cell, and the first Brillouin zone of the supercell (colored region).

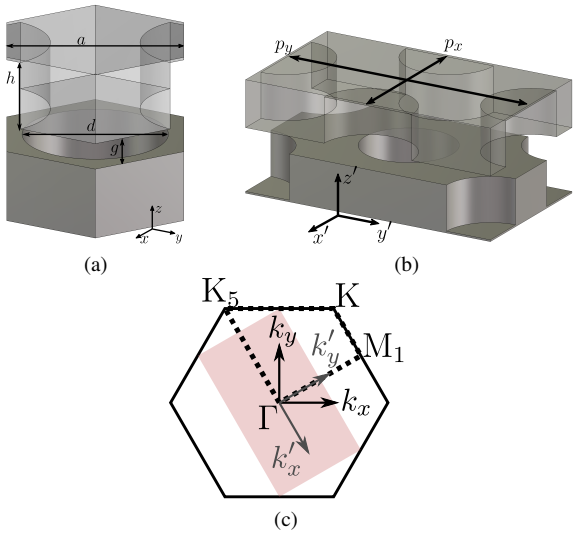

Fig. 2. Geometries of the glide-symmetric structure: (a) primitive unit cell and (b) the supercell. (c) The boundary of the first Brillouin zone (full line) and the irreducible Brillouin zone (dashed line) of the primitive cell, and the first Brillouin zone of the supercell (colored region).

TABLE I
USED SIMULATION PARAMETERS.

Variable	Meaning	Value
a	Distance across hexagon	8.7 mm
g	Gap between plates	0.05 mm
d	Radius of hole	$0.62a$
h	Depth of hole	$0.6a$

interest, as well as to select an appropriate supercell. The MMTMM requires a supercell to analyze hexagonal structures, as the used CST frequency domain solver with hexahedral meshing [16] needs the ports to be aligned with either one of the Cartesian axes for proper resolution of the port modes. To ensure that the solver can obtain the port modes accurately, it is recommended that the supercell boundaries are as uniform as possible.

The first periodic hexagonal structure analyzed is a mirror-symmetric PPW whose unit cell, depicted in Fig. 1(a), has a circular hole drilled in each of the plates. In the figure, the geometry parameters are the gap g, depth of hole h, width of hexagon a, and diameter of the hole d. The values of these parameters, used in the simulations, are reported in Table I. The boundary of the first Brillouin zone of the primitive cell is presented in Fig. 1(c) in solid line. In the same figure, the irreducible Brillouin zone is bounded by a dashed line and the first Brillouin zone of the supercell shown in Fig. 1(b) is colored in red. The periodicities of this rectangular supercell are $p_x = a$ and $p_y = 2\,a\cos(\pi/6)$.

The second analyzed structure is a glide-symmetric holey structure, with its primitive unit cell shown in Fig. 2(a). For this structure, the parameters in Table I result in a maximized stopband, starting at about 30 GHz. The supercell is shown in Fig. 2(b). The first Brillouin zone of the primitive cell and the irreducible Brillouin zone are bounded by full and dashed lines in Fig. 2(c). Since the structure does not possess 60° rotational

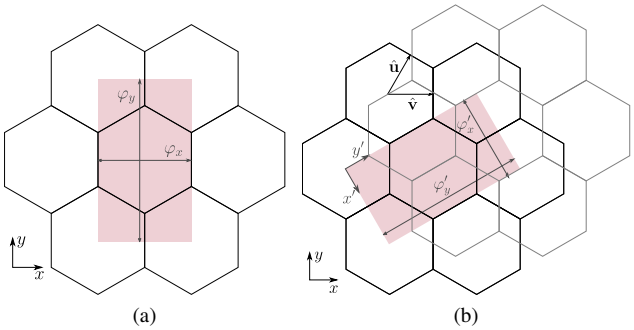

Fig. 3. Lattice of the (a) mirror-symmetric and (b) glide-symmetric hexagonal holey structures. The bottom part of the lattice is black and the top part is gray. The chosen supercell with the definition of phases is colored red

symmetry around the z-axis, its irreducible Brillouin zone is larger compared to the mirror-symmetric case in Fig. 1(c). The first Brillouin zone of the supercell is shown in red in Fig. 2(c). Since the supercell is rotated, its Brillouin zone is rotated as well and has its own pair of wavevectors, k'_x and k'_y, depicted in gray.

To further illustrate the selection of supercells, we present top-down views of the mirror-symmetric and glide-symmetric supercells in Fig. 3, where the 60°-rotation of the chosen glide-symmetric supercell compared to the mirror-symmetric primitive cell can be clearly appreciated. This rotation increases the homogeneity of the boundaries, since these coincide with the middle vertical planes of the holes. In the figure, the unit vectors $\hat{\mathbf{v}}$ and $\hat{\mathbf{w}}$ are defined. The top part of the glide-symmetric structure, depicted in gray, is obtained by a translation of $a/2$ in both directions. Moreover, the definition of phases across the supercell, φ_x and φ_y, is also shown in gray. The values of these phases at the edges of the irreducible Brillouin zone are listed for the mirror-symmetric and glide-symmetric structures in Tables II(A) and (B), respectively.

TABLE II
PHASES FOR THE EDGES OF THE IRREDUCIBLE BRILLOUIN ZONE

(A): Mirror-symmetric supercell

Point	φ_x	φ_y
Γ	0	0
M	0	2π
K	$\frac{2}{3}\pi$	2π

(B): Glide-symmetric supercell

Point	φ'_x	φ'_y
Γ	0	0
K_5	$-\frac{4}{3}\pi$	0
K	$-\frac{2}{3}\pi$	2π
M_1	0	2π

III. MODELLING METHODOLOGY

To analyze a unit cell with MMTMM, ports with N modes are defined at the boundaries of the unit cell. Using multiple modes is important to adequately model the near-field coupling between adjacent unit cells [9]. Open boundary conditions are established on the port planes. Once the generalized scattering matrix is obtained, it is transformed into the following multi-mode transfer matrix:

$$[\mathbf{T}] = \begin{bmatrix} [\mathbf{A}] & [\mathbf{B}] \\ [\mathbf{C}] & [\mathbf{D}] \end{bmatrix} \tag{1}$$

where the submatrices $[\mathbf{A}]$, $[\mathbf{B}]$, $[\mathbf{C}]$, and $[\mathbf{D}]$ are computed using [9]. We thus set up an eigenvalue problem as

$$[\mathbf{T}] \begin{bmatrix} \mathbf{V}_x \\ \mathbf{V}_y \\ \mathbf{I}_x \\ \mathbf{I}_y \end{bmatrix} = \begin{bmatrix} \lambda_x \mathbf{V}_x \\ \lambda_y \mathbf{V}_y \\ \lambda_x \mathbf{I}_x \\ \lambda_y \mathbf{I}_y \end{bmatrix} \tag{2}$$

where the vectors $\mathbf{V}_{x,y}$ and $\mathbf{I}_{x,y}$ are the effective voltages and currents of the N-port modes and

$$\lambda_\nu = \exp(-\mathrm{j}\varphi_\nu)\ . \tag{3}$$

Here, $\varphi_\nu = \mathbf{k}_\mathrm{t} \cdot \hat{\boldsymbol{\nu}} p_\nu$, where ν is either x or y, $\mathbf{k}_\mathrm{t}$ is the wavevector corresponding to a mode in the structure and p_ν is the spatial distance between the opposite ports of the supercell. Note that the obtained eigenvalue problem is not linear, but can be linearized [17]. The terms from (2) are first rearranged into

$$[\tilde{\mathbf{T}}] \begin{bmatrix} \mathbf{V}_x \\ \mathbf{I}_x \\ \mathbf{V}_y \\ \mathbf{I}_y \end{bmatrix} = \begin{bmatrix} \lambda_x \mathbf{V}_x \\ \lambda_x \mathbf{I}_x \\ \lambda_y \mathbf{V}_y \\ \lambda_y \mathbf{I}_y \end{bmatrix} \tag{4}$$

where the transfer matrix is permuted by $[\tilde{\mathbf{T}}] = [\mathbf{P}][\mathbf{T}][\mathbf{P}]^\mathrm{T}$, with $[\mathbf{P}]$ being a suitable permutation matrix. Then, the transfer matrix is subdivided into

$$[\tilde{\mathbf{T}}] = \begin{bmatrix} [\tilde{\mathbf{T}}_{xx}] & [\tilde{\mathbf{T}}_{xy}] \\ [\tilde{\mathbf{T}}_{yx}] & [\tilde{\mathbf{T}}_{yy}] \end{bmatrix} \tag{5}$$

and, after some matrix manipulations, the following eigenvalue problems are obtained:

$$\left([\tilde{\mathbf{T}}_{xx}] + [\tilde{\mathbf{T}}_{xy}][\mathbf{Q}_y][\tilde{\mathbf{T}}_{yx}]\right) \begin{bmatrix} \mathbf{V}_x \\ \mathbf{I}_x \end{bmatrix} = \lambda_x \begin{bmatrix} \mathbf{V}_x \\ \mathbf{I}_x \end{bmatrix} \tag{6}$$

$$\left([\tilde{\mathbf{T}}_{yy}] + [\tilde{\mathbf{T}}_{yx}][\mathbf{Q}_x][\tilde{\mathbf{T}}_{xy}]\right) \begin{bmatrix} \mathbf{V}_y \\ \mathbf{I}_y \end{bmatrix} = \lambda_y \begin{bmatrix} \mathbf{V}_y \\ \mathbf{I}_y \end{bmatrix} \tag{7}$$

where $[\mathbf{Q}_\nu] = \left(\lambda_\nu[\mathbf{I}] - [\tilde{\mathbf{T}}_{\nu\nu}]\right)^{-1}$. When dealing with rectangular unit cells, this approach enables the use of efficient eigenvalue algorithms. When the edge of the irreducible Brillouin zone is scanned, either one of the parameters λ_x or λ_y remains constant, or the eigenvalue problem (2) is already linear (when $\lambda_x = \lambda_y$). However, this is not the case for the $\overline{\mathrm{K}\Gamma}$ part of the mirror-symmetric hexagonal supercell, and for the $\overline{\mathrm{K}_5\mathrm{K}}$ in the glide-symmetric structure. In this case, the problem can be reformulated as a polynomial eigenvalue problem. Then, eigenvalues can be found through known routines, such as in [18].

IV. NUMERICAL RESULTS

First, we illustrate how to obtain the dispersion diagram of the primitive cell from that of the supercell. If a supercell is used, additional modes appear [15], [19], analogous to aliasing when undersampling a signal. For the mirror-symmetric structure, the supercell dispersion diagram is shown in Fig. 4(a). The figure shows the values of MMTMM and HFSS Eigenmode Solver (HFSS ES) [20] obtained with the supercell (dashed line) and the primitive cell (markers). According to [15], it is possible to identify which subset of supercell modes correspond to the primitive-cell modes by considering symmetry and comparing the Brillouin zones of the primitive cell and the supercell. Thus, for example, it can be observed that there is an additional mode in the $\overline{\Gamma\mathrm{M}}$ region starting at about 15 GHz that has an inversion symmetry with respect to that starting at 0 GHz. This mode and its continuation in other regions $\overline{\mathrm{MK}\Gamma}$ can then be labeled as "additional" modes. This identification of modes is clearly expected to agree with the comparison of the results of the HFSS ES for the primitive cell with those of the supercell. The result of this selection procedure can be seen in Fig. 4(b), which only shows the modes of the primitive cells. The vertical dash-dot line at M correspond to the phase shift of an evanescent mode with the attenuation presented in Fig. 4(c). Note that, although the structure does not possess a stopband in all directions (the propagating modes coincide at K), it can still block the propagation of waves in the $\hat{\mathbf{y}}$ direction. The fact that the results of the two methods are in excellent agreement in Fig. 4 can be taken as a validation of the MMTMM applied to hexagonal periodic structures.

Following a similar reduction procedure as above, Fig. 5(a) shows the dispersion diagram of the glide-symmetric primitive structure in Fig. 2(a). The primitive unit cell was simulated in the HFSS ES. Note that we plot the dispersion diagram along the boundaries of the irreducible Brillouin zone shown in Fig. 2(c). In Fig. 5(a), the MMTMM solutions are obtained by selecting a number of port modes whose cutoff frequencies are not much higher than the frequency range explored. In general, acceptable results have been obtained by retaining the first ten port modes (more discussion on the choice of these port modes can be found in [9]). The vertical lines in Fig. 5(a) at the two values of Γ (left: dashed-dotted line and right: dotted line) and M_1 (solid line with square/circle markers) correspond to the phase shifts of the stopband

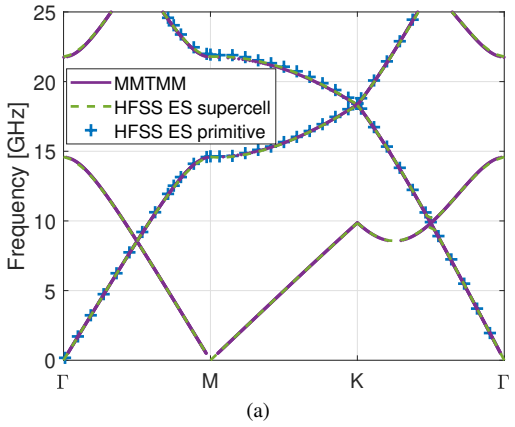

(a)

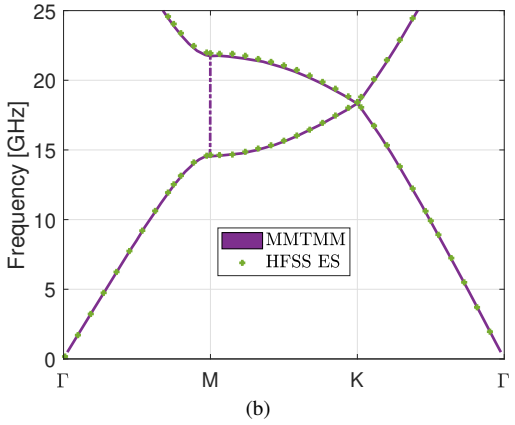

(b)

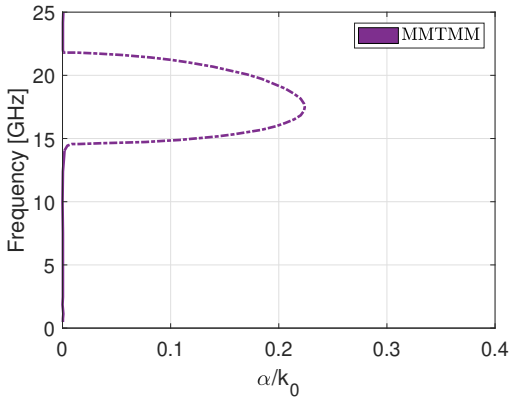

(c)

Fig. 4. Dispersion diagram of (a) the supercell and (b) the primitive unit cell of the mirror-symmetric structure. (c) Normalized attenuation in the $\overline{\Gamma \mathrm{M}}$ region (k_0 is the free space wavenumber). For the MMTMM, the first 6 modes were used.

modes calculated by the MMTMM. The MMTMM values of the normalized attenuation of these modes are depicted in Fig 5(b) as different purple lines. In the figure, both solid lines are obtained at M_1, but they are obtained by solving the eigenvalue problem for either $\overline{\mathrm{M}_1\Gamma}$ or $\overline{\mathrm{KM}_1}$. Thus, the normalized attenuation presented for the square markers is in the direction of $\overline{\mathrm{M}_1\Gamma}$, while for the circle markers it is in the direction of $\overline{\mathrm{KM}_1}$, as defined in Fig. 2(c). Unlike the mirror-symmetric structure, the glide-symmetric structure has

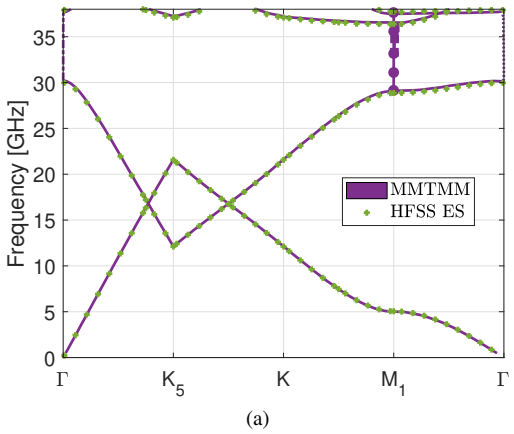

(a)

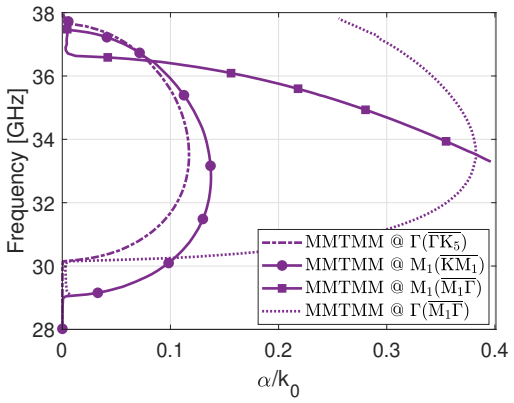

(b)

Fig. 5. (a): Dispersion diagram of the primitive glide-symmetric unit cell. (b): Normalized attenuation of the relevant modes in the first stopband.

a stopband in all directions.

A practical application of the results in Fig. 5(b) could be in the use of this periodic structure as EBG. The lower bound of the stopband is determined by the lower frequency of the evanescent mode at Γ while the upper bound is determined by the appearance of a second passband at M_1. The unit cell has a high degree of anisotropy in the stopband, as evidenced by the different values of the attenuation constant of the two evanescent modes at left/right Γ points. It suggests that the unit cell should be oriented in such a way that the incident wave travels in the direction of $\overline{\mathrm{M}_1\Gamma}$, thus maximizing the amount of attenuation. It should be noted that using this structure as an EBG may not be the most suitable choice, as the stopband and attenuation are not as high as those of rectangular glide-symmetric structures [10].

V. Conclusion

This paper has presented a modeling approach based on the multimodal transfer-matrix method (MMTMM) for hexagonal mirror and glide-symmetric structures. The implementation of the method was discussed, including the appropriate Brillouin zones, the use of the supercell, and the efficient solution of the eigenvalue problem. The results for the real part of the dispersion diagrams obtained with the MMTMM and a commercial eigenmode solver agree very well. Moreover, the

proposed method allows to evaluate also the modes attenuation in the stopband.

ACKNOWLEDGMENT

This publication is based upon work from COST Action SyMat (CA18223), supported by COST (European Cooperation in Science and Technology), by the Horizon Europe Research and Innovation Program under the GENIUS Project, Marie Skłodowska-Curie Grant under Agreement 101072560, and in part by the project PON Research and Innovation "Microwave Imaging and Detection powered by Artificial Intelligence for Medical and Industrial Applications (DM 1062/21)," funded by the Italian Ministry of University and Research (MUR). It is also supported by Unite! – University Network for Innovation, Technology and Engineering. The work of F. Mesa has been partially funded by the Grant PID2020-116739GB-I00 funded by MCIN/AEI/10.13039/501100011033.

REFERENCES

[1] O. Quevedo-Teruel, M. Ebrahimpouri, and M. Ng Mou Kehn, "Ultrawideband Metasurface Lenses Based on Off-Shifted Opposite Layers," *IEEE Antennas Wireless Propag. Lett.*, vol. 15, pp. 484–487, 2016.

[2] G. Valerio, F. Ghasemifard, Z. Sipus, and O. Quevedo-Teruel, "Glide-Symmetric All-Metal Holey Metasurfaces for Low-Dispersive Artificial Materials: Modeling and Properties," *IEEE Trans. Microw. Theory Techn.*, vol. 66, no. 7, pp. 3210–3223, 2018.

[3] A. Monje-Real, N. Fonseca, O. Zetterstrom, E. Pucci, and O. Quevedo-Teruel, "Holey Glide-Symmetric Filters for 5G at Millimeter-Wave Frequencies," *IEEE Microw. Wireless Compon. Lett.*, vol. 30, no. 1, pp. 31–34, 2019.

[4] B. Fischer and G. Valerio, "Quasi-Static Homogenization of Glide-Symmetric Holey Parallel-Plate Waveguides With Ultra-Wideband Validity," *IEEE Trans. Antennas Propag.*, vol. 70, no. 11, pp. 10 569–10 582, 2022.

[5] O. Quevedo-Teruel, Q. Chen, F. Mesa, N. J. Fonseca, and G. Valerio, "On the Benefits of Glide Symmetries for Microwave Devices," *IEEE J. Microw.*, vol. 1, no. 1, pp. 457–469, 2021.

[6] P. Crepeau and P. R. McIsaac, "Consequences of symmetry in periodic structures," *Proc. IEEE*, vol. 52, no. 1, pp. 33–43, 1964.

[7] A. Hessel, M. H. Chen, R. C. Li, and A. A. Oliner, "Propagation in periodically loaded waveguides with higher symmetries," *Proc. IEEE*, vol. 61, no. 2, pp. 183–195, 1973.

[8] Z. Sipus, K. Cavar, M. Bosiljevac, and E. Rajo-Iglesias, "Glide-Symmetric Holey Structures Applied to Waveguide Technology: Design Considerations," *Sensors*, vol. 20, no. 23, 2020.

[9] F. Mesa, G. Valerio, R. Rodriguez-Berral, and O. Quevedo-Teruel, "Simulation-Assisted Efficient Computation of the Dispersion Diagram of Periodic Structures: A comprehensive overview with applications to filters, leaky-wave antennas and metasurfaces," *IEEE Antennas Propag. Mag.*, vol. 63, no. 5, pp. 33–45, 2020.

[10] Q. Chen, F. Mesa, X. Yin, and O. Quevedo-Teruel, "Accurate Characterization and Design Guidelines of Glide-Symmetric Holey EBG," *IEEE Trans. Microw. Theory Techn.*, vol. 68, no. 12, pp. 4984–4994, 2020.

[11] S. Amari, R. Vahldieck, and J. Bornemann, "Accurate analysis of periodic structures with an additional symmetry in the unit cell from classical matrix eigenvalues," *IEEE Trans. Microw. Theory Techn.*, vol. 46, no. 10, pp. 1513–1515, 1998.

[12] M. Petek, J. Rivero, J. A. Vasquez-Tobon, G. Valerio, O. Quevedo-Teruel, and F. Vipiana, "Method of Moments for the Dispersion Modelling of Glide- Symmetric Periodic Structures," *IEEE Trans. Antennas Propag.*, in press.

[13] J. D. de Pineda, A. P. Hibbins, and J. R. Sambles, "Microwave edge modes on a metasurface with glide symmetry," *Phys. Rev. B*, vol. 98, p. 205426, Nov 2018.

[14] S. Yang, O. Zetterstrom, Z. Xue, F. Mesa, and O. Quevedo-Teruel, "Hexagonal higher-symmetric dielectric periodic structures for planar graded-index lenses," *Appl. Phys. Lett.*, vol. 123, no. 1, p. 011707, 07 2023.

[15] S. Yang, O. Zetterstrom, F. Mesa, and O. Quevedo-Teruel, "Dispersion Analysis of Metasurfaces With Hexagonal Lattices With Higher Symmetries," *IEEE J. Microw.*, vol. 3, no. 4, pp. 1154–1165, 2023.

[16] "CST Studio Suite 3D EM Simulation and Analysis Software." [Online]. Available: https://www.3ds.com/products-services/simulia/products/cst-studio-suite/

[17] F. Giusti, Q. Chen, F. Mesa, M. Albani, and O. Quevedo-Teruel, "Efficient Bloch Analysis of General Periodic Structures With a Linearized Multimodal Transfer-Matrix Approach," *IEEE Trans. Antennas Propag.*, vol. 70, no. 7, pp. 5555–5562, 2022.

[18] N. J. Higham, D. S. Mackey, and F. Tisseur, "The Conditioning of Linearizations of Matrix Polynomials," *SIAM J. Matrix Anal. Appl.*, vol. 28, no. 4, pp. 1005–1028, 2006.

[19] S. Yang, F. Mesa, O. Zetterstrom, S. Clendinning, and O. Quevedo-Teruel, "Understanding the Dispersion Diagrams of Two-Dimensional Supercells," in *2022 Microwave Mediterranean Symposium (MMS)*, 2022, pp. 1–4.

[20] "Ansys HFSS 3D Electromagnetic Field Simulator for RF and Wireless Design." [Online]. Available: https://www.ansys.com/products/electronics/ansys-hfss